DOI:10.1021/jf9033333

JOURNAL OF AGRICULTURAL AND FOOD CHEMISTRY
ARTICLE

Isoegomaketone Inhibits Lipopolysaccharide-Induced Nitric Oxide Production in RAW 264.7 Macrophages through the Heme Oxygenase-1 Induction and Inhibition of the Interferon-β-STAT-1 Pathway

Chang Hyun Jin,[†] Hyo Jung Lee,[‡] Yong Dae Park,[†] Dae Seong Choi,[†] Dong Sub Kim,[†] Si-Yong Kang,[†] Kwon-Il Seo,[§] and Il Yun Jeong*,[†]

[†]Advanced Radiation Technology Institute, Korea Atomic Energy Research Institute, Jeongeup, Jeonbuk, 580-185, Republic of Korea, [‡]Department of Life Science, Gwangju Institute of Science and Technology, Gwangju, 500-712, Republic of Korea, and [§]Department of Food and Nutrition, Sunchon National University, Sunchon 540-742, Republic of Korea

Isoegomaketone (IK) is an essential oil component of *Perilla frutescens* (L.) Britt., and there have been no studies investigating its biological activities. We found that IK inhibits lipopolysaccharide (LPS)-induced nitric oxide (NO) production in RAW 264.7 macrophages, and moreover, when IK was injected into animals prior to LPS administration, NO serum levels decreased in a dose-dependent manner. These results indicate that IK possesses anti-inflammatory activity both in vitro and in vivo. IK suppressed the phosphorylation of STAT-1 and the production of IFN-β. Treatment with IK also inhibited the activation of NF-κB and activator protein-1, but more IK was required for inhibition than for STAT-1 inhibition, indicating that downregulation of inducible nitric oxide synthase gene expression by IK is mainly attributed to the blockade of STAT-1 activation. Furthermore, IK also induced the expression of heme oxygenase-1 (HO-1) through the activation of nuclear factor E2-related factor 2. Treatment with SnPP, a selective inhibitor of HO-1, reversed the IK-induced suppression of STAT-1 phosphorylation and NO production. Taken together, IK isolated from *P. frutescens* inhibits NO production in LPS-treated RAW 264.7 macrophages through simultaneous induction of HO-1 and inhibition of the IFN-β−STAT-1 pathway.

KEYWORDS: Isoegomaketone; nitric oxide; lipopolysaccharide; STAT-1; heme oxygenase-1

INTRODUCTION

Lipopolysaccharide (LPS) is the major cell wall constituent of Gram-negative bacteria and is a potent activator of the immune system. Macrophages are major cellular targets for LPS action. LPS induces the production of nitric oxide (NO) and many pro-inflammatory cytokines in macrophages such as interleukin-6 (IL-6), tumor necrosis factor-α (TNF-α), and interleukin-1β (IL-1β) (*1*). NO has an important role in many diseases, such as atherosclerosis, inflammation, carcinogenesis, hypertension, obesity, and diabetes (*2*−*4*). NO is produced by nitric oxide synthase (NOS), which exists as three isoforms, endothelial NOS (eNOS), neuronal NOS (nNOS), and inducible NOS (iNOS). iNOS is expressed in response to LPS and is responsible for the excessive production of NO during the inflammatory process (*5*). Therefore, inhibition of NO production through inhibition of iNOS expression may be an effective strategy for the treatment of inflammatory diseases such as rheumatoid arthritis.

Heme oxygenase-1 (HO-1), the inducible isoform of heme oxygenase that catalyzes the degradation of heme into biliverdin, iron, and carbon monoxide (CO), is a novel enzyme with potent anti-inflammatory, antioxidant, and antiproliferative effects (*6*−*8*). HO-1 is involved in the inhibition of LPS-induced NO production (*9*,*10*). It appears that these physiological functions of HO-1 are mediated by the concerted actions of heme metabolites, including CO and bilirubin (*11*). The induction of the HO-1 gene is primarily regulated at the transcriptional level and is related to the transcription factor nuclear factor E2-related factor 2 (Nrf2) (*12*). Under normal conditions, Nrf2 is sequestered in the cytoplasm by its association with the keap1. When challenged by stimuli, Nrf2 dissociates from keap1, translocates into the nucleus, and elicits an antioxidant response (*13*).

Perilla frutescens (L.) Britt. is an annual herbaceous plant in the Lamiaceae family. Its leaves are used as food in Asian cuisines, and its seeds are used to make edible oil in Korea. It is also used in traditional Chinese medicine. Many studies regarding the pharmacological activities of *P. frutescens* have been conducted (*14*, *15*), and many compounds, such as rosmarinic acid, luteolin, apigenin, ferulic acid, (+)-catechin, and caffeic acid, have been isolated (*16*). Interestingly, there are many reports about the biological activities of rosmarinic acid (*17*) and luteolin (*18*). *P. frutescens* also contains several essential oil components including isoegomaketone (IK), and there are some reports about the anti-inflammatory activity of essential oil such as citral

*To whom correspondence should be addressed. Tel: +82-63-570-3150. Fax: +82-63-570-3159. E-mail: iyjeong@kaeri.re.kr.

 Published on Web 12/23/2009

(C) and phenylpropanoid (PP) (*19*, *20*). However, there are no studies regarding the biological activities of IK. In our previous report, we isolated IK from *P. frutescens* (*21*). In the present study, we investigated the suppressive effect of IK on LPS-induced NO formation in vitro and in vivo. We further examined the potential mechanisms by which IK inhibits LPS-induced NO production in RAW 264.7 macrophages and found that IK suppressed the activation of the IFN-β−STAT-1 pathway and induced HO-1 expression.

MATERIALS AND METHODS

Reagents. Dulbecco's modified Eagle's medium (DMEM) and fetal bovine serum (FBS) were purchased from Hyclone (Logan, UT). LPS, phenylmethylsulfonyl fluoride, sodium nitrite, dimethyl sulfoxide (DMSO), Griess reagent, and a protease inhibitor cocktail were purchased from Sigma-Aldrich (St. Louis, MO). Opti-MEMI medium, goat antirabbit IgG HRP-conjugated antibody, and Lipofectamine 2000 were purchased from Invitrogen (Carlsbad, CA). Tin protoporphyrin (SnPP), an HO-1 inhibitor, was purchased from Porphyrin Products Inc. (Logan, UT). The RNeasy kit was purchased from Qiagen (Valencia, CA). The EZ-Cytox Cell Viability assay kit was purchased from DAEIL lab (Korea). The Advantage RT-for-PCR kit was purchased from Clontech (Mountain View, CA). SYBR premix was purchased from Takara Bio Inc. (Japan). NP40 cell lysis buffer was purchase from Biosource (San Jose, CA). Rabbit polyclonal antibodies to IκBα, phospho-IκBα (Ser32), phosphor-Ikkβ (Ser181), iNOS, STAT-1, phosphor-STAT-1 (Tyr701), JNK, and phospho-JNK (Tyr185) were purchased from Cell Signaling Technology (Danvers, MA). Rabbit polyclonal antibodies against β-tubulin, HO-1, lamin B, and Nrf2 were purchased from Santa Cruz Biotechnology (Santa Cruz, CA). Enzyme-linked immunosorbent assay (ELISA) kits for MCP-1, IL-6, and IFN-β were purchased from R&D System (Minneapolis, MN). A NO assay kit was purchased from BioAssay Systems (Hayward, CA).

Animal Treatment. Animals were maintained in accordance with the guidelines of the Guide for the Care and Use of Laboratory Animals (Institute of Laboratory Animal Resources). Female BALB/c mice (4 weeks) were purchased from Orient Bio Inc. (Korea) and allowed to acclimate for 1 week prior to the beginning of the study. Mice were maintained in an air-conditioned room with lighting from 9 a.m. to 9 p.m. The room temperature (about 23 ± 2 °C) and humidity (approximately about 55 ± 10%) were controlled automatically.

Cell Culture. RAW 264.7 macrophage cells were cultured in DMEM supplemented with 10% FBS, penicillin (100 U/mL), and streptomycin (100 μg/mL) and incubated at 37 °C with 5% carbon dioxide.

Cytotoxicity Assay. To measure cell viability, we used the EZ-Cytox cell viability assay kit. Cells were cultured in a 96-well plate at a density of 2.0×10^5 cells/mL for 24 h. The cells were subsequently treated with various concentrations of IK for an additional 24 h. After the incubation period, 10 μL of the kit solution was added to each well and incubated for 4 h at 37 °C and 5% CO_2. The index of cell viability was determined by measuring formazan production with an ELISA reader at an absorbance of 480 nm. The reference wavelength was 650 nm.

Determination of NO Concentration. Nitrite in the cellular media was measured by the Griess method (*22*). The cells were cultured in a 96-well plate and treated with LPS (1 μg/mL) for 18 h. The cellular media were collected at the end of the culture period to assay for nitrite. Equal volumes of Griess reagent and cellular supernatant from each experimental condition were combined, and the absorbance of each sample was measured at 540 nm. The concentration of nitrite (μM) was calculated using a standard curve produced from a known concentration of sodium nitrite dissolved in DMEM. The results are presented as the means ± standard deviations (SDs) of four replicates of one representative experiment.

Serum Nitrite/Nitrate Measurement. Mice were randomly divided into six groups: (1) saline (i.p., $n = 5$), (2) LPS (10 mg/kg i.p., $n = 5$), (3) LPS plus IK (5 mg/kg i.p., $n = 5$), (4) LPS plus IK (10 mg/kg i.p., $n = 5$), (5) LPS plus IK (20 mg/kg i.p., $n = 5$), and (6) IK (20 mg/kg i.p., $n = 5$). IK was administered 1 h before LPS injection (i.p.). At 8 h after LPS treatment, a whole blood sample was taken by cardiac puncture after anesthetizing the mice with ether. The serum nitrite/nitrate concentration was determined using a NO assay kit according to the manufacturer's protocol.

Preparation of Cell Extracts and Western Blotting. Cells were washed once with cold phosphate-buffered saline (PBS) and harvested by pipetting. For whole-cell extract preparation, the cells were lysed in an NP40-based cell lysis buffer containing a protease inhibitor cocktail (Sigma) and phenylmethylsulfonyl fluoride (Sigma) for 30 min on ice. Nuclear and cytosolic extracts were prepared using a nuclear extraction kit (Sigma-Aldrich). The protein concentration of the cell lysate was determined using the Bio-Rad Protein Assay (Bio-Rad). Equal amounts of protein (50 μg) were loaded and electrophoresed on a 10% sodium dodecyl sulfate (SDS)−polyacrylamide gel and then transferred onto a nitrocellulose membrane (Hybond ECL Nitrocellulose, Amersham, United States). The membranes were washed once with a wash buffer (PBS, 0.05% Tween 20) and then blocked with a blocking buffer (PBS, 5% skim milk, 0.05% Tween 20) for 1 h. After they were blocked, the membranes were incubated with the relevant primary antibody overnight at 4 °C. Rabbit polyclonal antibodies to IκBα, phospho-IκBα (Ser32), phosphor-Ikkβ (Ser181), iNOS, STAT1, phosphor-STAT1 (Tyr701), JNK, and phospho-JNK (Y185) were diluted 1:1000, and the rabbit polyclonal anti-β-tubulin antibody was diluted 1:200 in blocking buffer. After they were incubated, the membranes were washed and subsequently incubated for 1 h at room temperature with goat antirabbit IgG HRP-conjugated secondary antibody diluted to 1:5000 in blocking buffer. The membranes were washed, and protein bands were detected by a chemiluminescence system (Amersham Pharmacia).

iNOS Protein Detection in LPS-Treated Mice. Lung tissues were homogenized in an NP40-based lysis buffer containing a protease inhibitor cocktail (Sigma) and phenylmethylsulfonyl fluoride (Sigma). The homogenates were then centrifuged three times at 13000*g* for 15 min. The supernatants were subjected to 10% SDS−polyacrylamide gel electrophoresis (PAGE) and then transferred onto a nitrocellulose membrane. The membranes were incubated with anti-iNOS and β-tubulin antiantibodies overnight at 4 °C. After they were incubated, the membranes were washed and incubated for 1 h at room temperature with goat antirabbit IgG HRP-conjugated secondary antibody. The membranes were washed, and protein bands were detected by a chemiluminescence system (Amersham Pharmacia).

Quantitative Real-Time Polymerase Chain Reaction (RT-PCR). Cells were cultured in a 100 mm Petri dish for 24 h (2×10^5 cell/mL). After stimulation with various concentrations of IK for 2 h, LPS (1 μg/mL) was added for 18 h. Total RNA from the cells was isolated using the RNeasy Kit according to the manufacturer's instructions. The Advantage RT-for-PCR kit was used for reverse transcription according to the manufacturer's protocol. A Chromo4 real-time PCR detection system (Bio-Rad) and iTaq SYBR^R Green Supermix (Bio-Rad) were used for RT-PCR amplification of iNOS, HO-1, and β-actin using the following conditions: 50 cycles of 94 °C for 20 s, 60 °C for 20 s, and 72 °C for 30 s. All reactions were repeated independently at least three times to ensure reproducibility of the results. Primers for iNOS, HO-1, and β-actin were purchased from Bioneer Corp. (Korea), and PCR was performed on cDNA using the following sense and antisense primers: iNOS, forward primer, 5′-TCCTACACCACACCAAACTGTGTGC-3′, and reverse primer, 5′-CTCCAATCTCTGCCTATCCGTCTC-3′; HO-1, forward primer, 5′-TACCTTCCCGAACATCGAC-3′, and reverse primer, 5′-GCATAAATTCCCACTGCCAC-3′; β-actin, forward primer, 5′-TGAGAGGGAAATCGTGCGTGAC-3′, and reverse primer, 5′-GCTCGTTGCCAATAGTGATGACC-3′. The specificity of the amplified PCR products was assessed by a melting curve analysis. The relative expression of target genes in comparison with the β-actin gene was evaluated by the comparative C_T threshold method using the Biorad software tool Genex-Gene Expression Macro (*23*).

Measurement of IFN-β and MCP-1 by ELISA. The quantities of IFN-β and MCP-1 in the culture medium were measured using an ELISA kit (R&D Systems) according to the manufacturer's protocol. The results are presented as the means ± SDs of three replicates of one representative experiment.

Luciferase Assay. Cells were cultured in a 6-well plate for 24 h at a density of 4×10^5 cells/mL. Transfection of the vectors was performed using Lipofectamine 2000 according to the manufacturer's instructions. The pNF-κB-*Luc* (Stratagene, La Jolla, CA) and pAP-1-*Luc* (Panomics, Fremont, CA) vectors were transfected using 5 μg of vector per well, including 1 μg/well of pRL-TK control reporter vector (Promega, Madison,

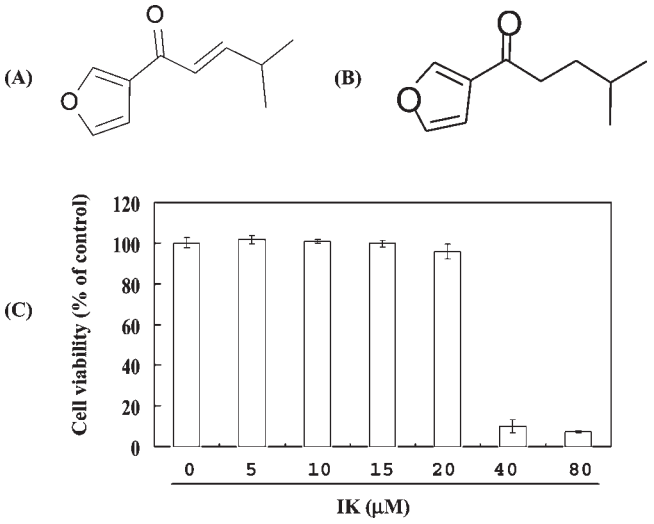

Figure 1. Chemical structure of IK, PK, and the effect of IK on cell viability. (**A**) Chemical structure of IK. (**B**) Chemical structure of PK. (**C**) Cell viability was determined by the EZ-Cytox cell viability assay kit. The cells were treated with various concentrations of IK for 24 h. After the incubation period, 10 μL of the kit solution was added to each well and incubated for an additional 4 h. The results are presented as the means ± SDs of four replicates of one representative experiment.

WI). After transfection, IK was added at various concentrations for 2 h, and the cells were treated with LPS at a concentration of 1 μg/mL for 24 h. The luciferase activity was measured using the Dual-luciferase Reporter Assay System (Promega).

Statistical Methods. Data are expressed as the mean ± standard error of the mean (SEM) of results obtained from the number of replicate treatments. Differences between data sets were assessed by one-way analysis of variance (ANOVA) followed by Newman−Keuls tests. A $p < 0.05$ was considered to be significant for all analyses.

RESULTS

Effect of IK on LPS-Stimulated NO Production in RAW 264.7 Macrophages. We first investigated whether IK suppressed NO production in RAW 264.7 macrophages. NO is a potentially toxic gas that is produced from the amino acid L-arginine through the enzymatic action of NOS. Appropriate levels of NO are important for organ protection, but excessive NO production is associated with many diseases including carcinogenesis, arthritis, and diabetes (*24*, *25*). NO production markedly increased from the basal level of 0.53 ± 0.09 to 20.42 ± 0.61 μM, after 18 h of incubation with LPS (1 μg/mL, **Figure 2A**). Interestingly, NO production decreased when IK was added to RAW 264.7 macrophages before LPS induction in a concentration-dependent manner (**Figure 2A**). The IC_{50} value was calculated at 6.9 μM. This inhibitory effect of IK was not due to cytotoxicity (**Figure 1C**). NOS has three isoforms, eNOS, nNOS, and iNOS. Among these, iNOS is induced in response to various inflammatory stimuli, such as LPS and pro-inflammatory cytokines, and is responsible for NO production during inflammation (*5*). To establish whether suppression of NO production by IK was due to inhibition of iNOS expression, we checked the protein and mRNA levels of iNOS. Western blot analyses showed that increases in this protein levels caused by LPS were attenuated in a dose-dependent manner after IK treatment (**Figure 2B**). In addition, RT-PCR analyses showed that iNOS mRNA levels were increased by LPS: This increase was significantly reduced by IK in a dose-dependent manner (**Figure 2C**). Our results indicated that IK inhibited LPS-induced NO production in RAW 264.7 macrophages via suppression of iNOS expression.

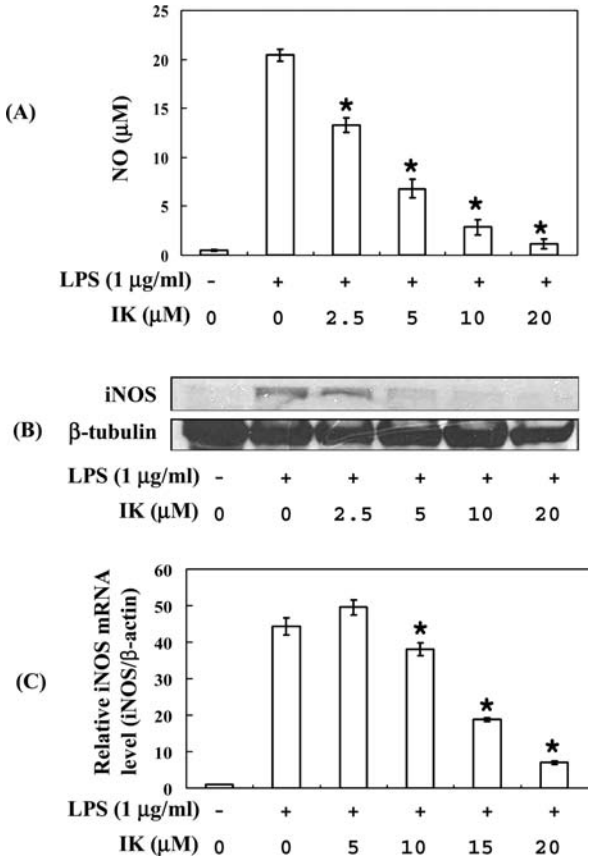

Figure 2. Effects of IK on NO production and iNOS expression levels in RAW 264.7 macrophages. RAW 264.7 macrophages were treated with the indicated concentrations of IK for 2 h prior to LPS addition (1 μg/mL) and were incubated for an additional 18 h. (**A**) Cellular media (100 μL) were mixed with equal volumes of Griess reagent. Nitrite levels were measured as an indicator of NO production as described in the Materials and Methods. Data shown are the means ± SDs ($n = 4$). *$P < 0.05$ vs the LPS-alone group. (**B**) Whole cell lysates were prepared, and the expression level of iNOS protein was measured by Western blot analysis. The result was confirmed by two independent experiments. (**C**) Total RNA was isolated, and the expression level of iNOS mRNA was measured by quantitative real-time PCR. Data shown are the means ± SDs ($n = 3$). *$P < 0.05$ vs LPS-alone-treated group.

Effect of IK on LPS-Stimulated NO Production in BALB/c Mice. We further examined whether IK inhibits NO production and increases iNOS protein levels in animal models. Mice were injected i.p. with IK (5, 10, and 20 mg/kg) for 1 h prior to injection of LPS and were then rested for an additional 8 h. Nitrite and nitrate (NOx) levels were significantly increased with LPS addition (63.90 ± 5.40 μM) as compared with those of mice injected with saline (9.85 ± 1.17 μM) or IK 20 mg/kg (16.86 ± 1.82 μM) (**Figure 3**). Interestingly, this increase was reduced after the addition of IK. Indeed, whereas iNOS protein levels in lung tissue increased after LPS injection (**Figure 3**), this effect was attenuated in the presence of IK. Therefore, these data suggest that IK suppresses NO production and iNOS expression both in vitro and in vivo.

Effect of IK on LPS-Stimulated IFN-β−STAT-1 Pathway in RAW 264.7 Macrophages. NO production in murine macrophages is not solely induced by LPS alone. LPS-induced NO production in RAW 264.7 macrophages can be enhanced by the addition of specific cytokines, such as TNF-α, IL-1β, and interferon-γ (IL-γ) (*26*). It has been reported that RAW 264.7 macrophages secrete IFN-α/β in response to LPS and that these

IFNs act through an autocrine/paracrine mechanism to induce iNOS expression (*26*). Moreover, it has been reported that STAT-1, a transcription factor, mediates the synergy between IFN- and LPS-induced iNOS expression in murine macrophages (*27*). Therefore, we examined the effect of IK on the IFN-β−STAT-1 pathway. When RAW 264.7 macrophages were stimulated with LPS (1 μg/mL), the levels of IFN-β continuously increased between 1 and 8 h: The increases were dramatically inhibited by IK (20 μM) treatment (**Figure 4A**). IK suppressed the production of IFN-β in a dose-dependent manner, with an IC_{50} value of 3.07 μM (**Figure 4B**). When RAW 264.7 macrophages were stimulated with LPS (1 μg/mL), STAT-1 phosphorylation was first detected at 1 h, peaked at 2 and 4 h, and then was followed by a subsequent decrease (**Figure 4C**). The phosphorylation levels of STAT-1 were reduced by treatment with IK in a dose-dependent manner (**Figure 4D**).

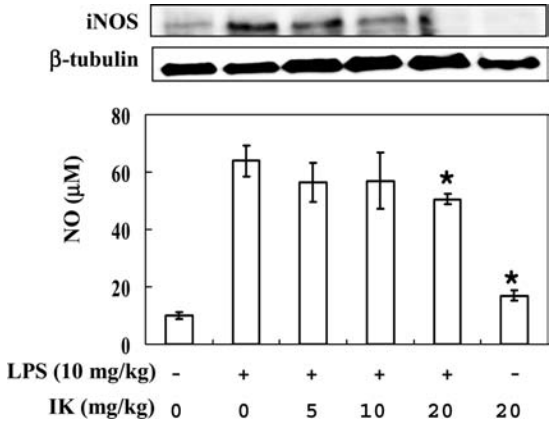

Figure 3. Effects of IK on serum NOx levels and iNOS expression in LPS-treated mice. Mice were treated with the indicated concentrations (5, 10, and 20 mg/kg) of IK for 1 h prior to LPS (1 μg/mL) injection. Mice were treated with LPS for 8 h. Serum NOx or iNOS protein levels in lung tissues were measured after anesthetizing the mice with ether. Data shown are the means ± SDs (n = 5). *P < 0.02 vs the LPS-alone group.

Up to this point, we could not determine whether IK inhibits STAT-1 phosphorylation directly or through its inhibition of IFN-β production. To solve this question, we used another stimulus, IFN-β, which does not exert its effect through TLR4 but rather through the IFN-β receptor. In our experiments, IFN-β could not induce NO production alone in RAW 264.7 macrophages, but it exhibited synergistic effects (when RAW 264.7 macrophages were treated with LPS and IFN-β, NO was produced faster and more than when cells were only treated with LPS) with LPS (data not shown). By contrast, with NO, IFN-β induced the production of monocyte chemotactic protein-1 (MCP-1) in RAW 264.7 macrophages alone, and this increase was reduced by IK treatment (**Figure 4E**). Therefore, IK suppressed the LPS-induced STAT-1 phosphorylation both directly and through its suppression of LPS-induced IFN-β production.

Effect of IK on LPS-Stimulated NF-κB and AP-1 Activation in RAW 264.7 Macrophages. NF-κB plays an important role in many aspects of human diseases and is an important transcription factor involved in iNOS gene expression (*28*). To investigate whether the effect of IK on iNOS expression is due to inhibition of NF-κB activation, we examined the transcriptional activity of NF-κB using a reporter gene assay. RAW 264.7 macrophages were transfected with the pNF-κB-*Luc* plasmid (containing repeats of NF-κB recognition sequences) and pRL-TK plasmid (containing cDNA encoding *Renilla* luciferase) and were then treated with IK for 2 h prior to the addition of LPS (1 μg/mL).

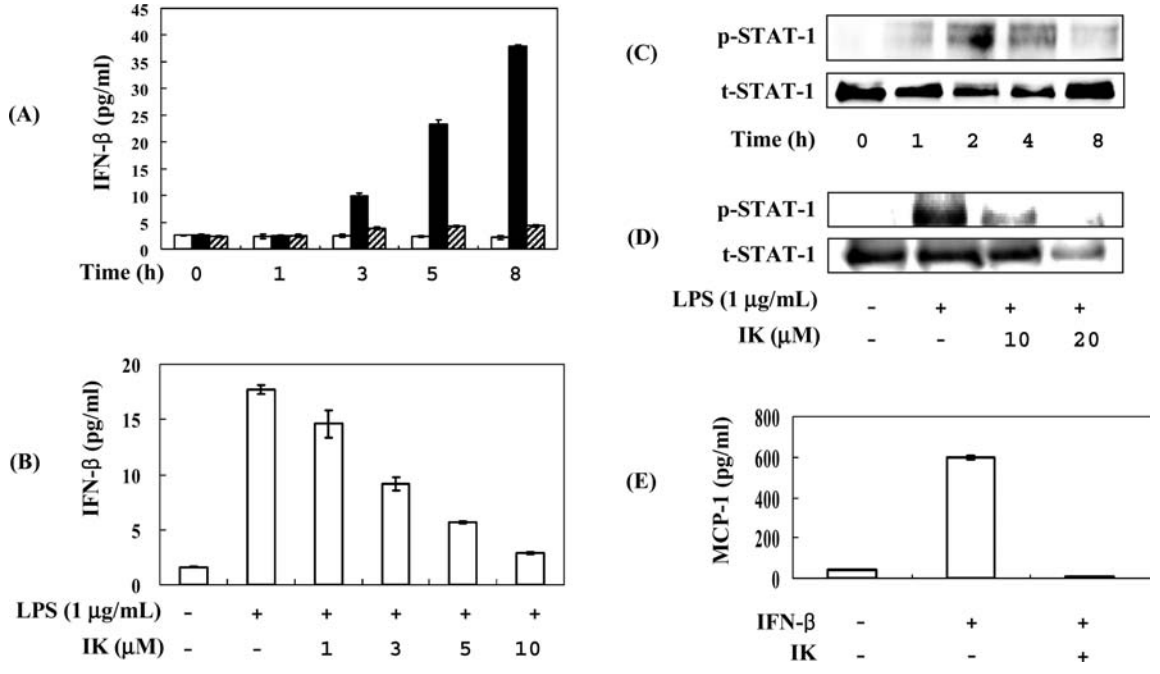

Figure 4. Effects of IK on IFN-β−STAT-1 pathways. (**A**) RAW 264.7 macrophages were treated with 20 μM IK for 2 h prior to LPS addition (1 μg/mL) and further incubated for the indicated time. The cellular medium was used for detecting IFN-β levels (white bars, none; black bars, LPS; and hatched bars, LPS + IK) using an ELISA kit. Data shown are the means ± SDs (n = 3). (**B**) RAW 264.7 macrophages were treated with IK for 2 h prior to LPS addition and further incubated for 5 h. Data shown are the means ± SDs (n = 3). (**C**) RAW 264.7 macrophages were treated with LPS (1 μg/mL) for the indicated times. Whole cell lysates (50 μg) were separated by SDS-PAGE, and protein levels were measured by Western blot analysis. (**D**) RAW 264.7 macrophages were treated with IK for 2 h prior to LPS addition and incubated for an additional 4 h. The whole cell lysates (50 μg) were used for Western blot analysis. (**E**) RAW 264.7 macrophages were treated with 20 μM IK for 2 h prior to the addition of IFN-β (100 units/mL) and incubated for an additional 8 h. MCP-1 levels were measured by ELISA using cellular medium. Data shown are the means ± SDs (n = 3).

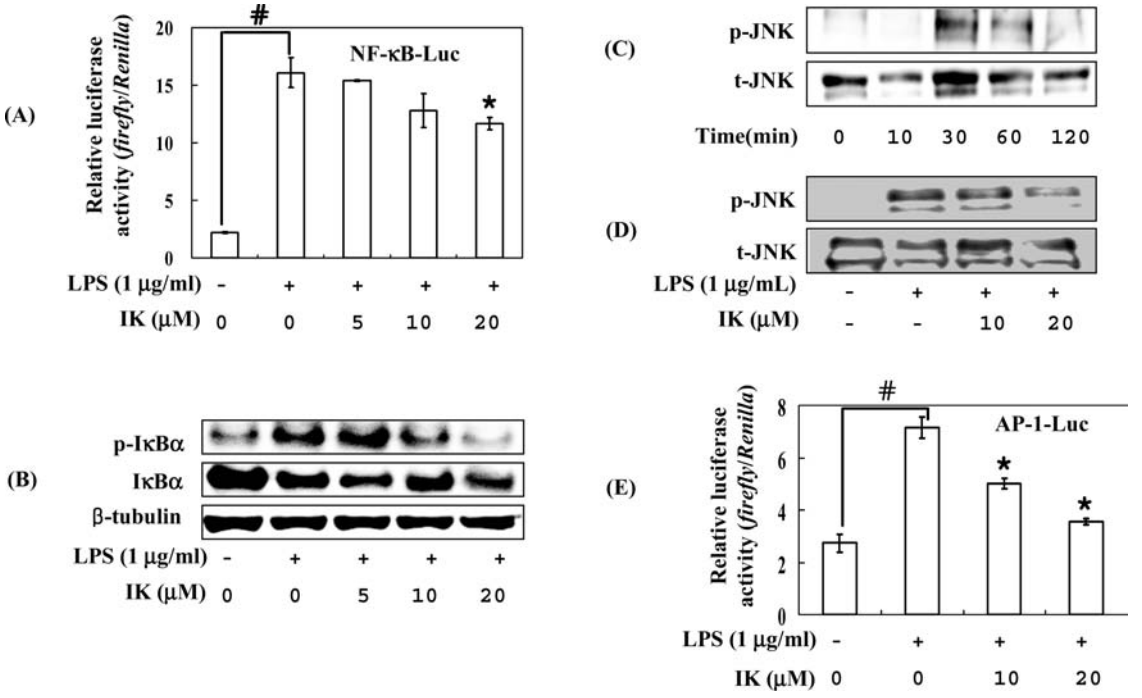

Figure 5. Effect of IK on the NF-κB and AP-1 pathway. (**A**) After transfection of pNF-κB-*Luc* and pRL-TK, RAW 264.7 macrophages were treated with IK prior to treatment with LPS and incubated for an additional 24 h. $^{\#}P < 0.005$ vs the media-alone group. $^{*}P < 0.05$ vs the LPS-alone group. (**B**) RAW 264.7 macrophages were treated with IK for 2 h prior to the addition of LPS and further incubated for 30 min. The whole cell lysates (50 μg) were used for Western blot analysis. (**C**) RAW 264.7 macrophages were treated with LPS (1 μg/mL) for the indicated time. The whole cell lysates (50 μg) were used for Western blot analysis. (**D**) RAW 264.7 macrophages were treated with IK for 2 h prior to the addition of LPS and further incubated for 30 min. The whole cell lysates (50 μg) were used for Western blot analysis. (**E**) After transfection of pAP-1-*Luc* and pRL-TK, RAW 264.7 macrophages were treated with IK prior to LPS addition and incubated for an additional 24 h. $^{\#}P < 0.005$ vs the media-alone group. $^{*}P < 0.05$ vs the LPS-alone group.

After 24 h, *Renilla* and firefly luciferase activities were measured and expressed as a ratio of firefly to *Renilla* luciferase activity. When LPS was added, the relative luciferase activity (firefly/*Renilla*) increased from 2.21 ± 0.07 to 16.08 ± 1.31. However, this increase was reduced in a dose-dependent manner by preincubation of IK (**Figure 5A**). NF-κB transcriptional activity is repressed by IκBα through the formation of a stable NF-κB$-$IκBα complex. When cells are stimulated by extracellular stimuli, such as LPS and pro-inflammatory cytokines, IκBα is phosphorylated by activated IKK-β (IκBα kinase) (*29*). Phosphorylated IκBα is ubiquitinated and degraded by the 26S proteasome (*30*), thereby releasing NF-κB dimers and allowing them to translocate to the nucleus. We investigated the effect of IK on IκBα phosphorylation. Stimulation by LPS increased phosphorylation of IκBα (**Figure 5B**) in RAW 264.7 macrophages, but this increased phosphorylation was inhibited by IK in a dose-dependent manner (**Figure 5B**).

LPS activates MyD88-dependent pathways, which lead to the activation of mitogen-activated protein kinases (MAPKs) such as c-Jun N-terminal kinase (JNK), extracellular regulated kinase (ERK), and p38. Among these kinases, JNK is involved in modulating iNOS expression in LPS-induced RAW 264.7 macrophages, but ERK and p38 are not (*10*). Therefore, we examined the effect of IK on JNK phosphorylation. When RAW 264.7 macrophages were stimulated with LPS (1 μg/mL), JNK phosphorylation peaked at 30 min and then decreased (**Figure 5C**). The levels of phosphorylation of JNK were reduced by IK treatment in a dose-dependent manner (**Figure 5D**). To confirm the effect of IK on JNK phosphorylation, we investigated the transcriptional activity of AP-1 using a reporter gene assay. RAW 264.7 macrophages were transfected with the pAP-1-*Luc* plasmid and pRL-TK plasmid and then treated with IK for 2 h prior to the addition of LPS (1 μg/mL). When LPS was added, the relative luciferase activity (firefly/*Renilla*) increased from 2.74 ± 0.34 to 7.16 ± 0.41. However, this increase was reduced in a dose-dependent manner by preincubation with IK (**Figure 5E**).

Taken together, IK suppressed LPS-induced NF-κB and AP-1 activation in LPS-induced RAW 264.7 macrophages. However, larger amounts of IK (about 2−4 times) are needed to inhibit NF-κB and AP-1 activation than are required to inhibit the IFN-β−STAT-1 pathway.

Effect of IK on HO-1 Induction and Nrf2 Activation in RAW 264.7 Macrophages. To investigate other factors responsible for the inhibition of IK on LPS-induced NO formation, we examined the effect of IK on HO-1 induction. HO-1 plays an important role in the regulation of inflammation. The structure of IK incorporates α,β-unsaturated ketone, a carbon−carbon double bond conjugated to a ketone (C_β=C_α−C=O). Previous reports have shown that these α,β-unsaturated carbonyl compounds have anti-inflammatory activity through HO-1 expression (*9*, *31*−*33*). Therefore, we also examined whether the suppressive effect of IK on LPS-induced NO production is mediated through HO-1 expression. Quantitative RT-PCR analysis indicated that treatment of IK (20 μM) considerably increased HO-1 mRNA levels in RAW 264.7 macrophages, showing a maximal increase after 4 h of IK treatment, and returned to baseline level after 12 h of treatment (**Figure 6A**). IK also led to an increase in HO-1 protein levels, showing a maximal increase after 4 h of treatment (**Figure 6B**). The rate of reduction in HO-1 protein levels was slower than that of HO-1 mRNA levels.

As discussed in the Introduction, Nrf2 is a transcription factor that leads to HO-1 induction by extracellular stimuli (*12*, *13*). To investigate the mechanism of HO-1 induction by IK in RAW 264.7 macrophages, we checked the effect of IK on the subcellular

localization of Nrf2. We prepared nuclear extracts and cytosolic fractions after IK treatment and measured Nrf2 levels by Western blot analysis. As shown in **Figure 6C**, IK increased Nrf2 protein levels in nuclear extracts, showed a maximal increase after 2 h of treatment, and returned to baseline levels after 8 h of treatment.

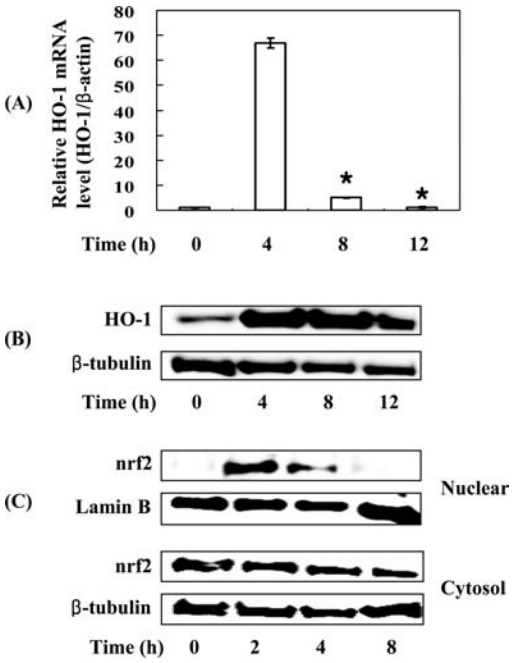

Figure 6. Effects of IK on HO-1 expression. RAW 264.7 macrophages were treated with 20 μM IK for the indicated time. (**A**) Total RNA was isolated, and the expression level of HO-1 mRNA was measured by quantitative real-time PCR. Data shown are the means ± SDs (n = 3). *P < 0.05 vs the LPS-alone-treated group. (**B**) The whole cell lysates (50 μg) were used for Western blot analysis. (**C**) Nuclear extracts (30 μg) and the cytosolic fraction (50 μg) were used for Western blot analysis.

IK treatment, however, did not increase Nrf2 protein levels in cytosolic fractions. These results indicated that IK increased the translocation of Nrf2 into the nucleus in RAW 264.7 macrophages and did not affect Nrf2 expression.

Role of HO-1 in the IK-Mediated inhibition of NO Production in LPS-Induced RAW 264.7 Macrophages. To investigate the possibility that HO-1 induction is responsible for the IK-mediated inhibition of LPS-induced NO production, cells were treated with LPS and IK in the presence of SnPP, a selective inhibitor of HO-1, and NO levels were measured. As shown **Figure 7A**, SnPP restored the IK-mediated suppression of NO production in a dose-dependent manner, while SnPP alone did not significantly affect LPS-stimulated NO production. Therefore, the inhibitory effect of IK on LPS-induced NO production is partially mediated by HO-1 induction.

To investigate how HO-1 is involved in the inhibition of LPS-induced NO production, we determined IFN-β production and STAT-1 phosphorylation in the presence of SnPP in LPS-induced RAW 264.7 macrophages. As shown in **Figure 7B**, SnPP could not restore the IK-mediated inhibition of IFN-β production, but it was able to restore the IK-mediated suppression of STAT-1 phosphorylation (**Figure 7C**). Therefore, HO-1 induced by IK inhibited the LPS-induced NO production through the inhibition of STAT-1 phosphorylation in RAW 264.7 macrophages.

DISCUSSION

Previously, we isolated IK in *P. frutescens* (L.) Britt. cv. Chookyoupjaso that was obtained by mutagenesis with γ-rays (*21*). *P. frutescens* (L.) Britt. is classified into five chemotypes according to the main components of the essential oils, such as perillaldehyde (PA), perillaketone (PK), elscholtziaketone (EK), C, and PP (*34*). IK and PK are biosynthesized from egomaketone (EGK), in a reaction that is controlled by gene *I* in *P. frutescens* (*35*). Many compounds isolated from *P. frutescens* were studied for their potential physiological activities (*17*, *18*), but there have been no reports regarding the biological activities of IK. In this study, we examined the anti-inflammatory activities

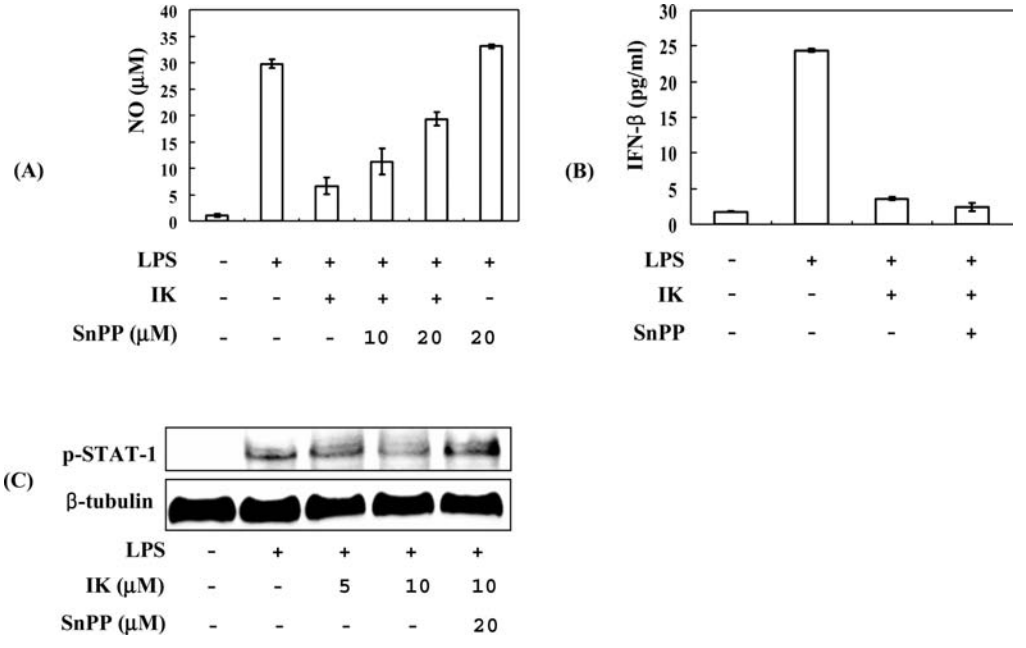

Figure 7. Involvement of HO-1 in IK-mediated anti-inflammation. (**A**) RAW 264.7 macrophages were treated with 20 μM IK and SnPP for 2 h prior to the addition of LPS (1 μg/mL) and further incubated for 18 h. Nitrite levels were measured by Griess reagent. (**B**) RAW 264.7 macrophages were treated with 20 μM IK and 20 μM SnPP for 2 h prior to the addition of LPS (1 μg/mL) and further incubated for 5 h. (**C**) RAW 264.7 macrophages were treated with IK and SnPP for 2 h prior to the addition of LPS (1 μg/mL) and further incubated for 4 h. The whole cell lysates (50 μg) were used for Western blot analysis.

of IK (**Figure 1A**) in RAW 264.7 macrophages. We found that IK suppressed LPS-induced NO production by inhibiting iNOS expression in RAW 264.7 macrophages (**Figure 2**) and mice (**Figure 3**). To our knowledge, this is the first report that describes the physiological activities of IK. We also isolated PK (**Figure 1B**) from *P. frutescens* (L.) Britt. cv. Chookyoupjaso and evaluated its effect on LPS-induced NO production, but its inhibitory activity (IC_{50} value for NO production was 271.8 μM) was much lower than that of IK. Therefore, we suggest that the α,β-unsaturated ketone of IK plays a very important role in anti-inflammatory activities.

LPS is a major component of the outer membrane of Gram-negative bacteria and induces cell types such as macrophages to secrete pro-inflammatory cytokines (*35*). LPS activates two branches of downstream signaling pathways, MyD88- and TRIF-dependent pathways, via the activation of TLR4 (*36*). Activation of MyD88- and TRIF-dependent pathways in TLR4 signaling is thought to be related to the induction of the early (MyD88) and late (TRIF) signaling pathways (*37*). MyD88 is a universal adaptor protein that is used by all TLRs (except TLR3) to activate the NF-κB transcription factor. The association of TLR4 and MyD88 recruits IRAK4 and TRAF6. TRAF6 activates TAK1, allowing NF-κB and AP-1 to translocate to nuclei (*36*). TRIF activates IFN-β promoters via TBK1 activation, a process that is independent of MyD88 (*38*). TRIF also activates NF-κB and AP-1 via TRAF6 or RIP1 (*36*, *38*). Importantly, LPS can activate NF-κB and AP-1 in MyD88-deficient mice (*35*).

In this study, we investigated the effect of IK on LPS-induced IFN-β-STAT-1 and NF-κB and AP-1 pathways (**Figures 4** and **5**). IK suppressed both IFN-β−STAT-1 pathways and NF-κB and AP-1 pathways, but more IK was required to inhibit NF-κB and AP-1 pathways as compared to IFN-β−STAT-1 pathways. Furthermore, we measured the IC_{50} values of IK for inhibition of IFN-β, MCP-1, and IL-6 levels in LPS-induced RAW 264.7 cells. The IC_{50} values are 3.1, 6.6, and 13.3 μM, respectively. MCP-1 production is partially dependent on the IFN-β−STAT-1 pathways, but IL-6 induction is not. Therefore, more IK is needed to inhibit MyD88-dependent pathways than is required to inhibit the TRIF-dependent pathway. Taking these data together, we suggest that the anti-inflammatory effect of IK is mainly mediated through the inhibition of IFN-β−STAT-1 pathways. The weak inhibition of NF-κB and AP-1 pathways by IK may be due to inhibition of activation of TRAF6 or RIP1 via TRIF. Further studies will be needed to understand how IK inhibits the IFN-β−STAT-1 pathways and to identify the main target molecule of IK.

Macrophages and endothelial cells express HO-1 in response to inflammatory stimuli. HO-1 decomposes heme into equimolar amounts of CO, iron, and biliverdin. Biliverdin is further converted to bilirubin, which is a potent endogenous antioxidant (*39*). CO derived from HO-1 catalysis exerts anti-inflammatory effects (*9*). In this study, we investigated the potential involvement of HO-1 in the anti-inflammatory activity elicited by IK. We found that IK increased HO-1 protein and mRNA expression levels through the translocation of Nrf2 into nuclei (**Figure 6**). The inhibitory activity of IK on LPS-induced NO production was attenuated by treatment with SnPP, a selective inhibitor of HO-1, in a dose-dependent manner (**Figure 7A**). Furthermore, SnPP decreased the inhibition of STAT-1 phosphorylation by IK but did not affect IFN-β production (**Figure 7B**,**C**). In a previous report, LPS-induced STAT-1 activation was prevented by HO-1 overexpression (*10*). Taken together, these results suggest that HO-1 is partially involved in the anti-inflammatory activity of IK through the inhibition of STAT-1 phosphorylation.

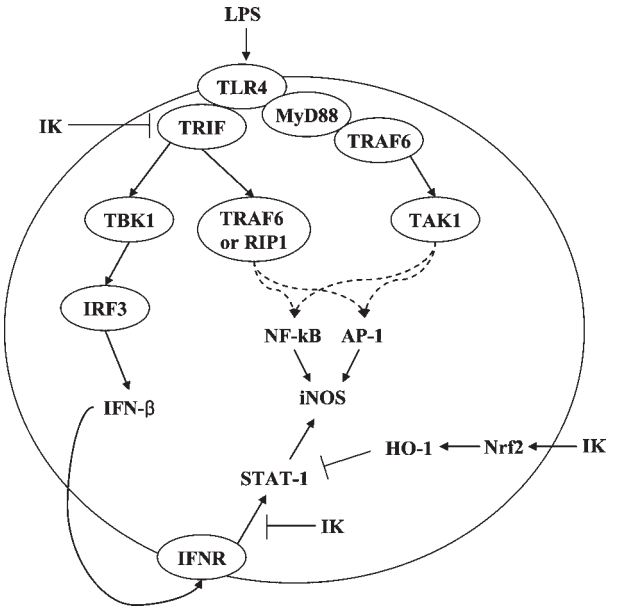

Figure 8. Possible model for the inhibition of iNOS or NO production by IK in LPS-induced RAW 264.7 macrophages. This model is based on the data in this report and previous reports. LPS activates Toll-like receptor 4 (TLR4), which causes activation of MyD88-dependent and TRIF-dependent pathways. IK inhibited the TRIF-dependent pathway and STAT-1 phosphorylation. IK also induces HO-1 expression through Nrf2.

We conclude that IK inhibited LPS-induced iNOS expression by inhibiting the IFN-β−STAT-1 pathways as well as inducing of HO-1, as depicted in **Figure 8**. Therefore, IFN-β−STAT-1 pathways may be major targets of IK.

LITERATURE CITED

(1) Pan, C. H.; Kim, E. S.; Jung, S. H.; Nho, C. W.; Lee, J. K. Tectorigenin inhibits IFN-gamma/LPS-induced inflammatory responses in murine macrophage RAW264.7 cells. *Arch. Pharm. Res.* **2008**, *31*, 1447–1456.

(2) Mordan, L. J.; Burnett, T. S.; Zhang, L. X.; Tom, J.; Cooney, R. V. Inhibitors of endogenous nitrogen oxide formation block the promotion of neoplastic transformation in C3H10T1/2 fibroblasts. *Carcinogenesis* **1993**, *14*, 1555–1559.

(3) Ohshima, H.; Bartsch, H. Chronic infections and inflammatory processes as cancer risk factors: Possible role of nitric oxide in carcinogenesis. *Mutat. Res.* **1994**, *305*, 253–264.

(4) Kröche, K. D.; Fensel, K.; Kolb-bachofen, V. Inducible nitric oxide synthase in human diseases. *Clin. Exp. Immunol.* **1998**, *113*, 147–156.

(5) Nathan, C.; Xie, Q. W. Nitric oxide synthases: Roles, tolls and controls. *Cell* **1994**, *78*, 915–918.

(6) Maines, M. D. Heme oxygenase: Function, multiplicity, regulatory mechanisms and clinical application. *FASEB J.* **1998**, *2*, 2557–2568.

(7) Yamada, N.; Yamaya, M.; Okinaga, S.; Nakyama, K.; Shibahara, S.; Sasaki, H. Microsatellite polymorphism in the heme oxygenase-1 gene promoter is associated with susceptibility to emphysema. *Am. J. Hum. Genet.* **2000**, *66*, 187–195.

(8) Tulis, D. A.; Durante, W.; Peyton, K. J.; Evans, A. J.; Schafer, A. I. Heme oxygenase-1 attenuates vascular remodeling following balloon injury in rat carotid arteries. *Atherosclerosis* **2001**, *155*, 113–122.

(9) Park, P. H.; Kim, H. S.; Jin, X. Y.; Jin, F.; Hur, J.; Ko, G.; Sohn, D. H. KB-34, a newly synthesized chalcone derivative, inhibits lipopolysaccharide-stimulated nitric oxide production in RAW264.7 macrophages via heme oxygenase-1 induction and blockade of activator protein-1. *Eur. J. Pharmacol.* **2009**, *606*, 215–224.

(10) Tsoyi, K.; Kim, H. J.; Shin, J. S.; Kim, D. H.; Cho, H. J.; Lee, S. S.; Ahn, S. K.; Yun-Choi, H. S.; Lee, J. H.; Seo, H. G.; Chang, K. C. HO-1 and JAK-2/STAT-1 signals are involved in preferential inhibition of iNOS over COX-2 gene expression by newly

synthesized tetrahydroisoquinoline alkaloid, CKD712, in cells activated with lipopolysacchride. *Cell. Signalling* **2008**, *20*, 1839–1847.
(11) Morse, D.; Choi, A. M. Heme oxygenase-1: The "emerging molecule" has arrived. *Am. J. Respir. Cell Mol. Biol.* **2002**, *27*, 8–16.
(12) Hanlon, P. R.; Webber, D. M.; Barnes, D. M. Aqueous extract from Spanish black radish (*Raphanus sativus* L. Var. niger) induces detoxification enzymes in the HepG2 human hepatoma cell line. *J. Agric. Food. Chem.* **2007**, *55*, 6439–6446.
(13) Li, W.; Kong, A. N. Molecular mechanisms of Nrf2-mediated antioxidant response. *Mol. Carcinog.* **2009**, *48*, 91–104.
(14) Ueda, H.; Yamazaki, M. Inhibition of tumor necrosis factor-alpha production by orally administering a perilla leaf extract. *Biosci., Biotechnol., Biochem.* **1997**, *61*, 1292–1295.
(15) Brochers, A. T.; Hackman, R. M.; Keen, C. L.; Stern, J. S.; Gershwin, M. E. Complementary medicine: A review of immunomodulatory effects of Chinese herbal medicines. *Am. J. Clin. Nutr.* **1997**, *66*, 1303–1312.
(16) Peng, Y.; Ye, J.; Kong, J. Determination of phenolic compounds in *Perilla frutescens* L. by capillary electrophoresis with electrochemical detection. *J. Agric. Food Chem.* **2005**, *53*, 8141–8147.
(17) Takeda, H.; Tsuji, M.; Inazu, M.; Eqashira, T.; Matsumiya, T. Rosmarinic acid and caffeic acid produce antidepressive-like effect in the forced swimming test in mice. *Eur. J. Pharmacol.* **2002**, *449*, 261–267.
(18) Selvendiran, K.; Koga, H.; Ueno, T.; Yoshida, T.; Maeyama, M.; Torimura, T.; Yano, H.; Kojiro, M.; Sata, M. Luteolin promotes degradation in signal transducer and activator of transcription 3 in human hepatoma cells: An implication for the antitumor potential of flavonoids. *Cancer Res.* **2006**, *66*, 4826–4834.
(19) Lee, H. J.; Jeong, H. S.; Kim, D. J.; Noh, Y. H.; Yuk, D. Y.; Hong, J. T. Inhibitory effect of citral on NO production by suppression of iNOS expression and NF-kappa B activation in RAW264.7 cells. *Arch. Pharmacal Res.* **2008**, *31*, 342–349.
(20) Diaz, A. M.; Abad, M. J.; Fernández, L.; Silván, A. M.; De, S. J.; Bermejo, P. Phenylpropanoid glycosides from *Scrophularia scorodonia*: In vitro anti-inflammatory activity. *Life Sci.* **2004**, *74*, 2525–2526.
(21) Park, Y. D.; Kang, M. A.; Lee, H. J.; Jin, C. H.; Choi, D. S.; Kim, D. S.; Kang, S. Y.; Byun, M. W.; Jeong, I. Y. Inhibition of an inducible nitric oxide synthase expression by a hexane extract from *Perilla frutescens* cv. Chookyoupjaso mutant induced by mutagenesis with gamma-ray. *J. Radiat. Ind.* **2009**, *3*, 13–18.
(22) Khan, M. S.; Priyadarshini, M.; Bano, B. Preventive effect of curcumin and quercetin against nitric oxide mediated modification of goat lung cystatin. *J. Agric. Food. Chem.* **2009**, *57*, 6055–6059.
(23) Canes, L.; Borghi, C.; Ciacci, C.; Fabbri, R.; Vergani, L; Gallo, G. Bisphenol-A alters gene expression and functional parameters in molluscan hepatopancreas. *Mol. Cell. Endocrinol.* **2007**, *276*, 36–44.
(24) Ruan, R. S. Possible roles of nitric oxide in the physiology and pathophysiology of the mammalian cochlea. *Am. N. Y. Acad. Sci.* **2002**, *962*, 260–274.
(25) Tylor, B. S.; Kion, Y. M.; Wang, Q. I.; Sharpio, R. A.; Billiar, T. R.; Geller, D. A. Nitric oxide down regulates hepatocyte-inducible nitric oxide synthase gene expression. *Arch. Surg.* **1997**, *1*, 1177–1182.
(26) Jacobs, A. T.; Ignarro, L. J. Lipopolysaccharide-induced expression of interferon-beta mediates the timing of inducible nitric-oxide synthase induction in RAW 264.7 macrophages. *J. Biol. Chem.* **2001**, *276*, 47950–47957.
(27) Kovarik, P.; Stoiber, D.; Novy, M.; Decker, T. Stat1 combines signals derived from IFN-gamma and LPS receptors during macrophage activation. *EMBO J.* **1998**, *17*, 3660–3668.
(28) Diaz-Guerra, M. J.; Velasco, M.; Martin-Sanz, P.; Bosca, L. Evidence for common mechanisms in the transcriptional control of type II nitric oxide synthase in isolated hepatocytes. Requirement of NF-kappaB activation after stimulation with bacterial cell wall products and phorbol esters. *J. Biol. Chem.* **1996**, *271*, 30114–30120.
(29) Zandi, E.; Chen, Y.; Karin, M. Direct phosphorylation of I kappaB by IKKαand IKKβ: Discrimination between free and NF-kB-bound substrate. *Science* **1998**, *281*, 1360–1363.
(30) Chen, Z.; Hagler, J.; Palombella, V. J.; Melandri, F.; Scherer, D.; Ballard, D.; Maniatis, T. Signal-induced site-specific phophorylation targets I kappa B alpha to the ubiquitin-proteasome pathway. *Genes Dev.* **1995**, *9*, 1586–1597.
(31) Tanaka, H.; Nakamura, S.; Onda, K.; Tazaki, T.; Hirano, T. Solfacone, an anti-ulcer chalcone derivative, suppresses inflammatory crosstalk between macrophages and adipocytes and adipocyte differentiation: Implication of heme oxygenase-1 induction. *Biochem. Biophys. Res. Commun.* **2009**, *381*, 566–571.
(32) Lee, S. H.; Kim, J. Y.; Seo, G. S.; Kim, Y. C.; Sohn, D. H. Isoliquiritigenin, from *Dalbergia odorifera*, up-regulates anti-inflammatory heme oxygenase-1 expression in RAW264.7 macrophages. *Inflamm. Res.* **2009**, *58*, 257–262.
(33) Jeong, G. S.; Lee, D. S.; Kim, Y. C. Cudratricusxanthone A from *Cudrania tricuspidata* suppresses pro-inflammatory mediators through expression of anti-inflammatory heme oxygenase-1 in RAW264.7 macrophages. *Int. Immunopharmacol.* **2009**, *9*, 241–246.
(34) Nishizawa, A.; Hoda, G.; Tabata, M. Determination of final steps in biosynthesis of essential oil components in *Perilla frutescens*. *Planta Med.* **1989**, *55*, 251–253.
(35) Kawai, T.; Adachi, O.; Ogawa, T.; Takeda, K.; Akira, S. Unresponsiveness of MyD88-deficient mice to endotoxin. *Immunity* **1999**, *11*, 115–122.
(36) Kawai, T.; Akira, S. TLR signaling. *Cell Death Differ.* **2006**, *13*, 816–825.
(37) Covert, M. W.; Leung, T. H.; Gaston, J. E.; Baltimore, D. Achieving stability of lipopolysaccharide-induced NF-kB activation. *Science* **2005**, *309*, 1854–1857.
(38) Sato, S.; Sugiyama, M.; Yamamoto, M.; Watanabe, Y.; Kawai, T.; Takeda, K.; Akira, S. Toll/IL-1 receptor domain-containing adaptor inducing IFN-β (TRIF) associates with TNF receptor-associated factor 6 and TANK-binding kinase 1, and activates two distinct transcription factors, NF-kB and IFN-regulatory factor-3, in the Toll-like receptor signaling. *J. Immunol.* **2003**, *171*, 4304–4310.
(39) Ryter, S. W.; Alam, J.; Choi, A. M. Heme oxygense-1/carbon monoxide: From basic science to therapeutic application. *Physiol. Rev.* **2006**, *86*, 583–650.

Received for review September 22, 2009. Revised manuscript received November 24, 2009. Accepted December 7, 2009. This work was supported by a grant from Agricultural R&D Promotion Center, Korea Rural Economic Institute.